Automated Detection and Analysis of Dermoscopic Structures on Dermoscopy Images

Maryam Sadeghi
Computing Science
Simon Fraser University
Burnaby, BC, Canada
msa68@sfu.ca

Tim K. Lee
Cancer Control Research
BC Cancer Agency,
Vancouver, BC, Canada
tlee@bccrc.ca

Stella Atkins
Computing Science
Simon Fraser University
Burnaby, BC, Canada
stella@sfu.ca

1. PROBLEM AND MOTIVATION

Melanoma, a cancerous lesion in the pigment-bearing basal layers of the epidermis, is the most deadly form of skin cancer, yet treatable via excision if detected early. In the last three decades, a rising incidence of malignant melanoma has been observed [1]. Because of the lack of adequate therapies for metastatic melanoma, the best treatment is still early diagnosis and prompt surgical excision of the primary cancer [15, 19]. There is, therefore, a demand to develop computer-aided diagnostic systems to facilitate the early detection of melanoma. Dermoscopy, also known as epiluminescence microscopy, is an in-vivo noninvasive imaging method that is useful for the early recognition of malignant melanoma [19, 18, 17]. The various types of pigmented skin lesions, with particular regard to the differentiation between benign and malignant melanocytic lesions, can be determined through detection of specific dermoscopic features. In all methods, dermatologists look for presence of specific visual features for making a diagnosis. Then, if present, these features are analyzed for irregularities and malignancy. In this work we translated the clinical criteria to mathematical concepts to be used by computers for computer-aided diagnosis of skin cancers.

Pigment Network: A pigment network can be classified as either *Typical* or *Atypical*, where a working definition of a typical pigment network (TPN) is "a light-to-dark-brown network with small, uniformly spaced network holes and thin network lines distributed more or less regularly throughout the lesion and usually thinning out at the periphery" [3]. For an atypical pigment network (APN) we use the working definition "a black, brown or gray network with irregular holes and thick lines" [3]. The goal is to automatically classify a given image to one of three classes: *Absent*, *Typical*, or *Atypical*. Figure 2 exemplifies these 3 classes. We use these definitions to subdivide the structure into the darker mesh of the pigment network (which we refer to as the 'net') and the lighter colored areas the net surrounds (which we refer to as the 'holes'). After identifying these substructures we use the definitions above to derive a several structural, geometric, chromatic and textual features suitable for classification.

Figure 1: The 3 classes of the dermoscopic structure pigment network: *Absent*, *Typical* and *Atypical* respectively.

Streaks: Streaks is a term used interchangeably with radial streaming or pseudopods. Radial streaming is a linear extension of pigment at the periphery of a lesion radially arranged linear structures in the growth direction, and pseudopods represent finger-like projections of dark pigment (brown to black) at the periphery of the lesion [7]. In order to ensure accurate recognition, streaks are numerated only when at least 3 near linear and parallel structures are clearly visible [24]. Streaks are *local* dermoscopy features of skin lesions, however they can correlate with a *global* pattern of skin lesions called a starburst pattern if symmetrically arranged over the entire lesion.

Mathematical definition of streaks: The above clinical definition is translated to mathematical concepts with justified parameters to be captured by image processing techniques: 1) Streaks are 3 or more linear structures co-radially oriented in the boundary which is a contour with the thickness equal to 1/3 of the minor axis of the lesion. 2) Streaks

(a) (b) (c)

Figure 2: Examples of absent, regular and irregular streaks. (a) shows a lesion without streaks (*Absent*). (b) illustrates a lesion with a complete symmetric regular streaks pattern called *starburst* (*Present*), and in (c), a melanoma lesion with irregular streaks is shown (*Present*).

are darker than their neighborhood. 3) Streaks are shorter than the 1/3 of the minor axis of the lesion and they should be longer than one percent of the major axis. 4) Streaks do not branch and their curvature is smaller than one. Figure 2 shows examples of lesions with no streaks (*Absent*), regular (*Present*), and irregular (*Present*) streaks. Figure 2-a shows *Absent, 2-b* shows a starburst or complete pattern with regular streaks, and Figure 2-c shows a lesion with irregular streaks and partial pattern.

2. PREVIOUS WORK

The automated detection of pigment network has received some recent attention [10, 6, 8, 23, 20]. Although these studies have certainly made significant contributions, there has yet to be a comprehensive analysis of pigment network detection on a large number of dermoscopic images under 'real-world' conditions. All work to date has either: 1) not reported quantitative validation [10, 9]; 2) validated against a small ($n < 100$) number of images[6]; 3) only considered or reported results for the 2-class problem (e.g. *Absent/Present* rather than *Absent/Typical/Atypical*)[2, 6, 8, 23]; 4) not explicitly identified the location of the network [2]; or 5) has made use of unrealistic exclusion criteria and other manual interventions [23].

The automatic detection of streaks has only recently been investigated [5, 16]. Streaks on dermoscopy images usually are difficult to detect since they are not perfect linear structures, but often fuzzy and low-contrast oriented intensities. Furthermore, streaks may have unpredictable spatial distribution (partial pattern) with just a few streaks lines in a small region of a lesion. Therefore, it is not easy to detect them using general oriented pattern analysis. Mirzaalian et al. [16] have used a machine-learning approach for classifying streaks in dermoscopic images. Although the methodology is interesting, it, unfortunately, has been tested on a small number (99) of dermoscopic images with wide exclusion criteria. It is not clear how the method generalizes to all conditions of dermoscopic images captured in a dermatologist clinic. This paper presents an effective method for pigment network segmentation and classification, which is validated on a large ($n = 436$) 'real-world' dataset.

3. APPROACH AND UNIQUENESS

3.1 Pigment Network Detection

After pre-processing and segmenting lesions from the normal skin [25], 'hole detector' is employed to generate a 'hole mask' indicating the pixels belonging to the holes of the pigment network. Next, a 'net mask' is created, indicating the pixels belonging to the net of the pigment network. We then use these masks to compute a varity of features including structural (which characterizes shape), geometric (which characterizes distribution and uniformity), chromatic and textural features. These features are fed into a classifier to classify unseen images.

3.1.1 Hole Detection:

After a pre-processing step, sharp changes of intensity are detected using the Laplacian of Gaussian (LOG) filter. The result of this edge detection step is a binary image which is subsequently converted into a graph to find meshes or cyclic

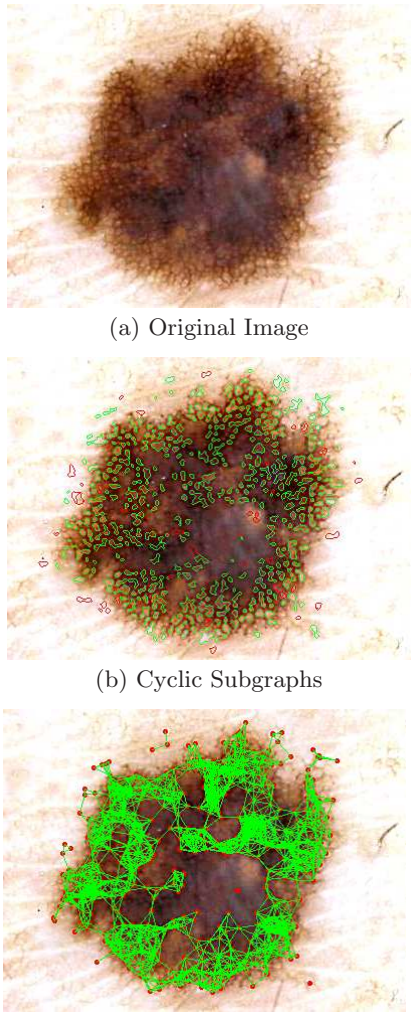

(a) Original Image

(b) Cyclic Subgraphs

(c) *Present*

Figure 3: Results of applying our approach to a dermoscopic image; (a) shows a skin lesion, (b) shows cyclic subgraphs, the green meshes represent potential holes of the pigment network and red meshes could not pass the test of belonging to the pigment network, and (c) visualizes the pigment network over the image.

structures of the lesion. After finding loops or cyclic subgraphs of the graph, noise or undesired cycles are removed and a graph of the pigment network is created using the extracted cyclic structures. According to the density of the pigment network graph, the given image is classified into *Present* or *Absent*.

In order to visualize the graph of a pigment network, we created a new higher-level graph whose nodes are centers of the meshes belonging to the pigment network (green meshes). Feagure 3 shows results of pigment network hole detection visualized by graph representation.

3.1.2 Net Detection:

In order to identify the net of a pigment network, we apply the Laplacian of Gaussian (LoG) filter to the green channel of the image. The LoG filter identifies high frequency components of an image and therefore makes an ideal net

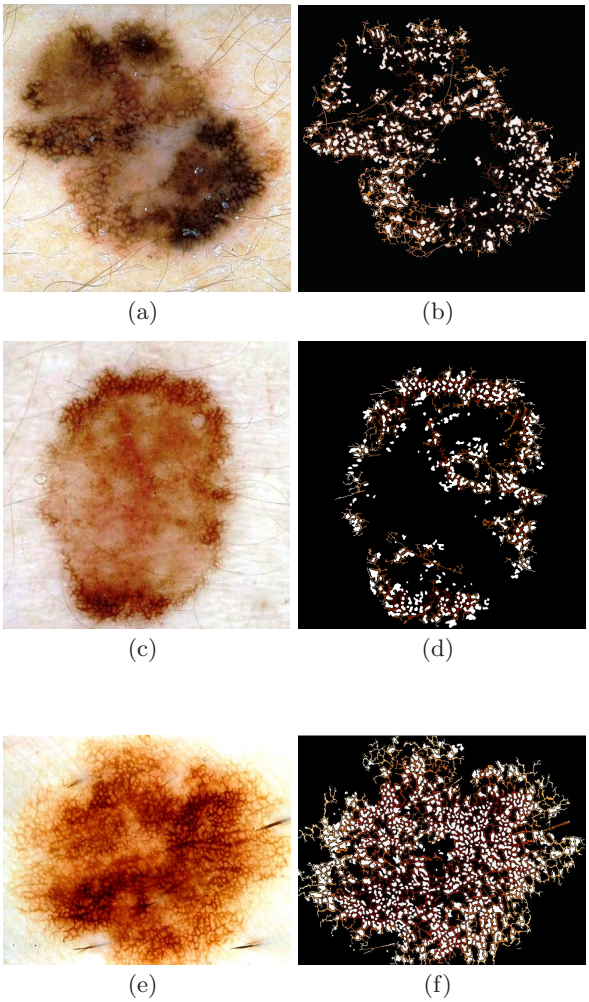

Figure 4: Three images of the image set along with the result of the method in the second column: the top row shows an APN and its result is shown in the second coloum. The mi, APN, and TPN. The bottom row shows their corresponding pigment networks.

detector. The major issue with applying this operator is that its response is strongly dependent on the relationship between the frequency of the structures and the size of the Gaussian kernel used. We used $\sigma = 0.15$, which is an appropriate value for images of the two atlases used in our experiment [4, 24], however it can be tuned for a given imageset according to scale and magnification. We then threshold the filter response, resulting in a 'net mask' which indicates which pixels belong to the net of the the pigment network. Figure 4 shows the final result of pigment network detection.

3.2 Streaks Detection

First the lesion is segmented and the orientation of the lesion is found, and the image is rotated to align the major axis horizontally since the major axis represents the lesion growth direction. Then, to have a relatively uniform image size, the lesion is re-sized so that its major axis occupies 500 pixels. Finally, the image is enhanced using a simple 3x3 high pass filter that removes the low frequency noise [21]. To get a single plane luminance image, the given RGB image is converted to the L*a*b color-space and L*, is used for the rest of our analysis (Figure 5-b). Then, multi-scale Laplacian of Gaussian is applied to detect dermoscopy structures with Gaussian-like profile. After finding linear structures, the orientation flow of the image is analyzed to determine the orientation of detected objects in the orientation flow to select linear structures of candidate streaks. Finally, chromatic and textural features of detected line segments are used to classify the lesions into *Absent* or *Present* images. An overview of our method is given in Figure 5.

Blob detection using LOG: Since streaks are linear structures with Gaussian-like profiles, we detect them using Laplacian of Gaussian (LOG). To capture objects of different sizes a multi-scale approach is necessary. Figure 5-d and 5-e show the LOG responses at two different scales of $hsize_k = 3, 9$ respectively.

Estimating orientation: After finding linear structures by LOG, the orientation estimation is performed using the Averaged Squared Gradient Flow (ASGF) algorithm [14]. The algorithm starts by computing the gradients $G_x(i,j)$ and $G_y(i,j)$ at each pixel (i,j) in image I. For doubling the angle and squaring the length in ASGF, the gradient vector is converted to *polar* coordinates. The image is divided into blocks of size W=16. For each block, the local orientation centered at pixel (i,j) is estimated and averaged. To reduce the effect of noise on the estimated orientation, a low-pass filter (Gaussian) is used to modify the local ridge orientation. Now, the local orientation and its reliability (the coherence of the squared gradients given by [14]) can be computed at pixel (i,j). This algorithm results in a smooth intensity flow orientation over the image (shown in Figure 5-f), and Figure 5-g shows the reliability map of the orientation estimation in the example image.

Estimating ridge frequency: After finding the local orientation and averaging for image blocks, the local ridge frequency is estimated by rotating the block so that the ridges are vertical. Then, the columns are projected down to find peaks. The frequency of ridges can be calculated by dividing the distance between the first and last peaks by (number of peaks -1), and finally the median frequency is computed over all the blocks in the image. The final result of frequency estimation for all blocks of our example image (5-d) is shown in Figure 5-h.

Enhancing orientation image: From [12], a Gabor filter with tuned ridge frequency and orientation, can remove the noise efficiently while preserves true ridges and valleys. The even-symmetric Gabor filter has the general form of $g(x,y;f,\theta,\sigma) = \exp\left(-\frac{x'^2+y'^2}{2\sigma^2}\right)\cos(2\pi f x')$, $x' = x\cos\theta + y\sin\theta$, and $y' = -x\sin\theta + y\cos\theta$, where σ is the sigma of the Gaussian kernel in the filter, and f and θ are the corresponding median ridge frequency over the image and local orientation respectively. The result of this step is shown in Figure 5-i. Figure 5-j shows the binary image of the enhanced orientation created by thresholding (1 for ridges and 0 for valleys), and Figure 5-k is created from (j) and (g) by removing pixels with $reliability \leq 50\%$. The skeleton of the

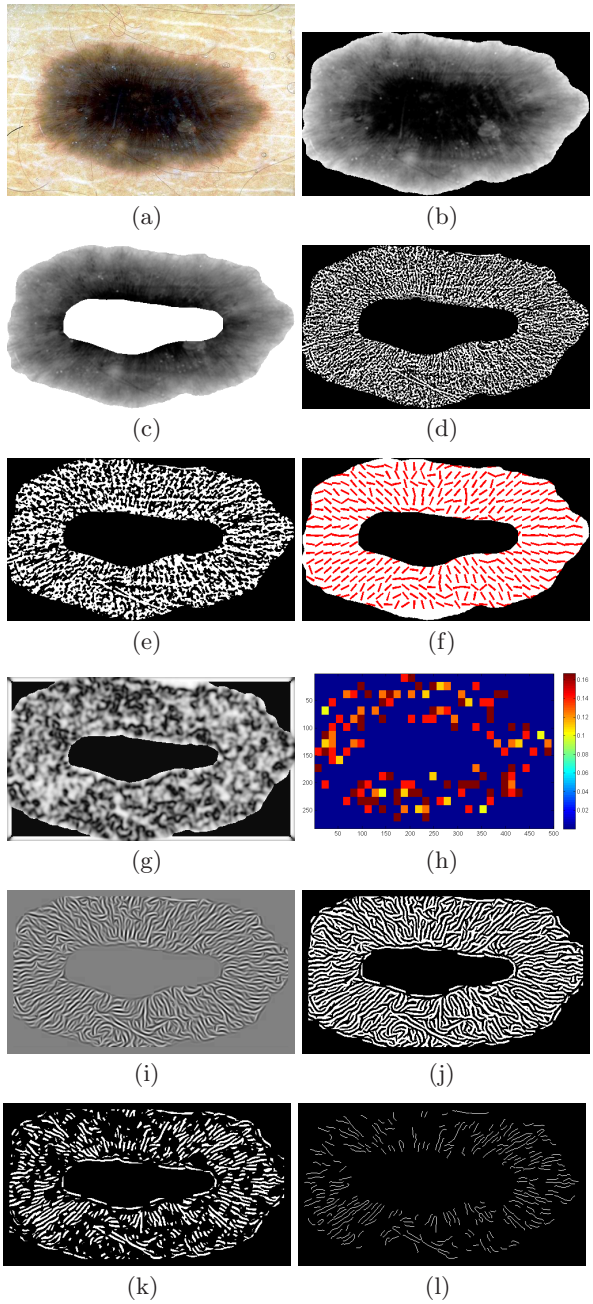

Figure 5: Steps of our streaks detection method. (a) shows a lesion with regular streaks and (b) illustrates the result of segmentation re-orientated and sharpening in the L* channel. (c) illustrates the region of interest that will be processed to find streaks. (d), and (e) show the LOG filter responses in the two scales $hsize_k = 3, 9$ respectively. In (f), the directional flow is plotted with red lines for $hsize_k = 9$, and (g) shows the reliability of estimation. The median frequency of the parallel pattern, illustrated in (h), is used in Gabor filters applied to enhance the estimated orientation shown in (i). (j) shows the binary image of the enhanced orientation with 1 for ridges and 0 for valleys. (k) is created from (g) and (j) by removing pixels with $reliability \leq 50\%$ and skeleton of the result is shown in (l) as detected candidate streaks structures.

result is shown in (l) as detected linear structures in the image. These line segments will be used for feature extraction in the next step.

Figure 6 demonstrates our streak detection method qualitatively. Figures 6-a, illustrates an *absent* image and its results is shown in 6-b. Figure 6-c shows a starburst lesions (*regular* streaks) with its streaks detected in Figure 6-d. A melanoma with *irregular* streaks and its result are shown in 6-e and 6-f.

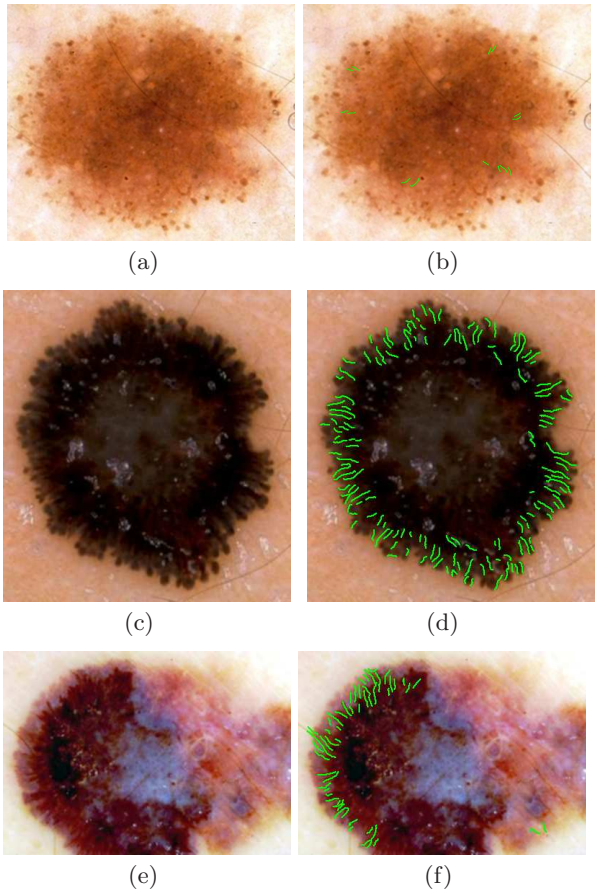

Figure 6: Qualitative results of streak detection. (a) illustrates an *absent* lesion and its results is shown in (b). (c) and (g) are starburst lesions with *regular* streaks. Their regular streaks are shown in (f) and (h). Two melanomas with *irregular* streaks are shown in the third row, (i) and (k), with their corresponding results in (j) and (l).

3.3 Classification

After segmenting the dermoscopy structures, pigment network and streaks, we extract a set of features for each based on the clinical definition of the structure.

For pigment network we used the 69 structural, geometric, chromatic and textual features [22].

For streaks classification, based on our mathematical definitions of streaks, we propose a new set of 12 features

Absent-Typical-Atypical Classification				
	Precision	Recall	F-measure	N
Absent	0.905	0.950	0.927	161
Typical	0.787	0.792	0.790	154
Atypical	0.750	0.694	0.721	121
Weighted Avg	**0.820**	**0.823**	**0.821**	436
Di Leo et al. [8]	0.709	0.711	0.709	436
Absent-Present Classification				
Absent	0.893	0.932	0.912	161
Present	0.959	0.935	0.947	275
Weighted Avg	**0.935**	**0.933**	**0.934**	436
Di Leo et al. [8]	0.875	0.876	0.875	436

Table 1: Comparing accuracy, precision, recall and f-measure of our proposed features with Di Leo et al.'s features using the same set of 436 images. The last three rows summarize the results from previous work on different image sets.

called *STR* which includes three structural, six chromatic, and 3 textural characteristics of candidate streaks. In *STR*, **Structural** set includes the number of candidate streaks in the image, average number of pixels of candidate streaks, and the ratio of the streaks size to the lesion size in pixels; **Chromatic** set consists of the mean, standard deviation and reciprocal of coefficient of variation (mean/stdev) of candidate streaks in L* and S, and std of H; and **Textural** features are energy, contrast, and homogeneity of candidate streaks. We have also used common color and texture features [22] of the lesion itself (called *LCT*). *LCT* includes the following 13 features: The mean, standard deviation and reciprocal of coefficient of variation (mean/stdev) of values in H, S, and V from HSV and L* of L*a*b*, and four of the classical Gray-level co-occurrence matrix based texture measures; energy, contrast, correlation, and homogeneity [22].

These features are fed into a classifier so that new images can be classified. We employ the WEKA's [11] implementation SimpleLogistic which uses a powerful boosting algorithm LogitBoost.

4. RESULTS

Using ten-fold cross-validation, we evaluated our proposed approach on streak and pigment network detection in separate experiments.

We applied our pigment network detection method to a set of 436 dermoscopic images taken from two atlases of dermoscopy [4, 24]. Our dataset consists of 161 *Absent*, 154 *Typical*, and 121 *Atypical* lesions. We compute results for both the 3-class (*Absent*, *Typical* or *Atypical*) and 2-class problems (*Absent*, *Present*). Table 1 summarizes these results.

For streaks detection, we used a set of 300 dermoscopy images, including 105 *absent* and 195 *present* from [4, 24]. Corrupted images due to the acquisition parameters such as lighting and magnification, partial lesions (entire lesion was not visible), or lesions occluded with an unreasonable amount of either oil or hair are excluded. Using the L channel of the L*a*b* colour channel as the luminance image for streak detection, we obtained the best performance for both data sets. For 300 images, accuracy of *Absent*/*Present* classification using L* is 85%, with AUC of 90.5%. In the second experiment, 200 images (100 *starburst*, and 100 *non-starburst*) are used to evaluate the performance of our method on the starburst detection problem. We achieved the accuracy of 81.5% and AUC of 87.7% using 10-fold cross validation. Table 2 reports detailed results of our evaluation.

Experiment	N	Ftrs	Prc.	Rec	AUC
Abs/Pres	300	LCT	0.712	0.722	0.779
		STR	0.835	0.837	0.901
		LCT+STR	**0.85**	**0.87**	**0.905**
Starburst	200	LCT+STR	**0.815**	**0.815**	**0.877**

Table 2: Evaluation of the proposed method. This table shows results of *LCT* (first row) and *STR* (second row) separately and combined (third row) for the multi-scale analysis on the L* on classifying N lesions with (*Present*) and without (*Absent*) streaks. The last row shows the evaluation of the method on another set of 200 images ($N = 200$) for finding starburst pattern. The last column (AUC) shows the Area Under ROC curve.

5. CONCLUSION AND FUTURE WORK

We have developed an algorithm to locate and classify pigment network structure in dermoscopy images using graph analysis. We have also presented an automatic approach for detection of radially oriented streaks on real dermoscopic images, using techniques based on ridge and valley detection used in fingerprint image recognition. We demonstrated that the proposed approaches can detect two important structures in dermoscopy images and visualize them. Therefore, they can improve the accuracy of melanoma detection in computer-aided skin lesion analysis. Furthermore, since the proposed method locates the structures and provides a qualitative analysis, they can be used to highlight suspicious areas for expertsS diagnosis and for visualization and training purposes.

6. REFERENCES

[1] American cancer society. 2009 cancer facts and figures, 2009. [online] accessed on Jan 5, 2011 , `http://www.melanomafoundation.org/facts/statistics.htm`.

[2] M. Anantha, R. Moss, and W. Stoecker. Detection of pigment network in dermatoscopy images using texture analysis. *Computerized Medical Imaging and Graphics*, 28(5):225–234, 2004.

[3] G. Argenziano, H. Soyer, et al. Dermoscopy of pigmented skin lesions: results of a consensus meeting via the internet. *Journal of the American Academy of Dermatology*, 48(5):679–693, 2003.

[4] G. Argenziano, H. P. Soyer, V. De Giorgio, D. Piccolo, P. Carli, M. Delfino, A. Ferrari, V. Hofmann-Wellenhof, D. Massi, G. Mazzocchetti, M. Scalvenzi, and I. H. Wolf. *Interactive Atlas of Dermoscopy (Book and CD-ROM)*. Edra medical publishing and new media, 2000.

[5] G. Betta, G. Di Leo, G. Fabbrocini, A. Paolillo, and M. Scalvenzi. Automated application of the 7-point checklist diagnosis method for skin lesions: Estimation

of chromatic and shape parameters. In *Proceedings of the IEEE Instrumentation and Measurement Technology Conference*, pages 1818–1822, 2005.

[6] G. Betta, G. Di Leo, G. Fabbrocini, A. Paolillo, and P. Sommella. Dermoscopic image-analysis system: estimation of atypical pigment network and atypical vascular pattern. In *MeMea 2006.*, pages 63–67. IEEE Computer Society, 2006.

[7] R. Braun, H. Rabinovitz, M. Oliviero, A. Kopf, and J. Saurat. Dermoscopy of pigmented skin lesions. *J. of the American Academy of Dermatology*, 52(1):109–121, 2005.

[8] G. Di Leo, C. Liguori, A. Paolillo, and P. Sommella. An improved procedure for the automatic detection of dermoscopic structures in digital ELM images of skin lesions. In *IEEE VECIMS*, pages 190–194, 2008.

[9] S. Fischer, J. Guillod, et al. Analysis of skin lesions with pigmented networks. In *Proc. Int. Conf. Image Proce.*, pages 323–326, 1996.

[10] M. Fleming, C. Steger, et al. Techniques for a structural analysis of dermatoscopic imagery. *Computerized medical imaging and graphics*, 22(5):375–389, 1998.

[11] M. Goebel. A survey of data mining and knowledge discovery software tools. *ACM SIGKDD Explorations Newsletter*, 1(1):20–33, 1999.

[12] L. Hong, Y. Wan, and A. Jain. Fingerprint image enhancement: Algorithm and performance evaluation. *IEEE Transactions on Pattern Analysis and Machine Intelligence*, 20:777–789, 1998.

[13] R. Johr. Dermoscopy: alternative melanocytic algorithmsŮthe ABCD rule of dermatoscopy, Menzies scoring method, and 7-point checklist. *Clinics in dermatology*, 20(3):240–247, 2002.

[14] M. Kass and A. Witkin. Analyzing oriented patterns. *Computer Vision, Graphics, and Image Processing*, 37(3):362–385, 1987.

[15] H. Kittler, H. Pehamberger, K. Wolff, and M. Binder. Diagnostic accuracy of dermoscopy. *The lancet oncology*, 3(3):159–165, 2002.

[16] H. Mirzaalian, T. Lee, and G. Hamarneh. Learning features for streak detection in dermoscopic color images using localized radial flux of principal intensity curvature. In *In IEEE workshop on Mathematical Methods for Biomedical Image Analysis (IEEE MMBIA)*, pages 97–101, 2012.

[17] F. Nachbar, W. Stolz, T. Merkle, A. Cognetta, and T. Vogt. The abcd rule of dermatoscopy: High prospective value in the diagnosis of doubtful melanocytic skin lesions. *Journal of the American Academy of Dermatology*, 30(4):551–559, 1994.

[18] H. Pehamberger, M. Binder, A. Steiner, and K. Wolff. In vivo epiluminescence microscopy: improvement of early diagnosis of melanoma. *Journal of Investigative Dermatology*, 100:356S–362S, 1993.

[19] H. Pehamberger, A. Steiner, and K. Wolff. In vivo epiluminescence microscopy of pigmented skin lesions. i. pattern analysis of pigmented skin lesions. *Journal of the American Academy of Dermatology*, 17(4):571–583, 1987.

[20] M. Sadeghi, M. Razmara, M. Ester, T. Lee, and M. Atkins. Graph-based pigment network detection in skin images. In *Proc. of SPIE Vol*, volume 7623, 2010.

[21] M. Sadeghi, M. Razmara, T. Lee, and M. Atkins. A novel method for detection of pigment network in dermoscopic images using graphs. *Computerized Medical Imaging and Graphics*, 35(2):137–143, 2011.

[22] M. Sadeghi, M. Razmara, P. Wighton, and S. Lee, T.and Atkins. Modeling the dermoscopic structure pigment network using a clinically inspired feature set. In *Medical Imaging and Augmented Reality*, volume 6326 of *Lecture Notes in Computer Science*, pages 467–474. Springer, 2010.

[23] B. Shrestha, J. Bishop, K. Kam, X. Chen, R. Moss, W. Stoecker, S. Umbaugh, R. Stanley, M. Celebi, A. Marghoob, et al. Detection of atypical texture features in early malignant melanoma. *Skin Research and Technology*, 16(1):60–65, 2010.

[24] H. Soyer, G. Argenziano, et al. Dermoscopy of pigmented skin lesions. an atlas based on the consensus net meeting on dermoscopy 2000. *Milan Edra*, 2001.

[25] P. Wighton, M. Sadeghi, T. Lee, and M. Atkins. A fully automatic random walker segmentation for skin lesions in a supervised setting. In *MICCAI (1)*, pages 1108–1115, 2009.